Proton–hydride tautomerism in hydrogen evolution catalysis

Luis M. Aguirre Quintana[a,b], Samantha I. Johnson[a,b], Sydney L. Corona[a,b], Walther Villatoro[a,b], William A. Goddard III[a,b], Michael K. Takase[a,b], David G. VanderVelde[a,b], Jay R. Winkler[a,b,1], Harry B. Gray[a,b,1], and James D. Blakemore[a,b,c,1]

[a]Beckman Institute, California Institute of Technology, Pasadena, CA 91125; [b]Division of Chemistry and Chemical Engineering, California Institute of Technology, Pasadena, CA 91125; and [c]Department of Chemistry, University of Kansas, Lawrence, KS 66044

Contributed by Harry B. Gray, April 17, 2016 (sent for review February 4, 2016; reviewed by Alexander Miller and David Milstein)

Efficient generation of hydrogen from renewable resources requires development of catalysts that avoid deep wells and high barriers. Information about the energy landscape for H_2 production can be obtained by chemical characterization of catalytic intermediates, but few have been observed to date. We have isolated and characterized a key intermediate in $2e^- + 2H^+ \rightarrow H_2$ catalysis. This intermediate, obtained by treatment of Cp*Rh(bpy) (Cp*, η^5-pentamethylcyclopentadienyl; bpy, κ^2-2,2′-bipyridyl) with acid, is not a hydride species but rather, bears [η^4-Cp*H] as a ligand. Delivery of a second proton to this species leads to evolution of H_2 and reformation of η^5-Cp* bound to rhodium(III). With suitable choices of acids and bases, the Cp*Rh(bpy) complex catalyzes facile and reversible interconversion of H^+ and H_2.

rhodium | pentamethylcyclopentadienyl | catalysis | proton reduction | hydrogen evolution

Sustainable and economically competitive production of hydrogen (H_2) as a fuel depends on the development of new molecules and materials that catalyze conversion of protons and electrons into H_2 with high rates and minimal energy input (1). Platinum fulfills these latter requirements but fails the economic test. Rational design of new catalysts that overcome these challenges hinges on a detailed understanding of the elementary chemical reaction steps involved in H–H bond formation (2). Notably, catalysis with a molecular cobalt complex, a [BF_2]-bridged cobaloxime, has been shown by kinetics and modeling to proceed by protonation of a Co^{II}–H complex to yield H_2 (3). However, most intermediates in H_2 evolution elude detection, limiting insight into the bond-breaking and -making processes involved in catalysis (4). In recent work, we have descended to the second row of group 9 in the periodic table to enable observation and isolation of catalytic intermediates.

We report here on our investigations of $[Cp^*Rh^{III}(diimine)L]^{2+}$ (Cp*, η^5-pentamethylcyclopentadienyl) complexes that evolve hydrogen catalytically on reduction. In early work, Kölle and Grätzel (5) found that H_2 is evolved on reduction at pH < 2 in an aqueous photochemical system, and Deronzier and coworkers (6) observed electrochemical H_2 evolution at pH 1. Of interest here is our finding that H_2 is evolved electrochemically in acetonitrile solutions of $[Cp^*Rh^{III}(diimine)L]^{2+}$ with tosic acid serving as the proton source (7). The η^5-Cp* ligand imparts high stability and solubility to these catalysts (8). Not surprisingly, then, they have been used widely for catalysis of redox transformations, including reduction of NAD^+ to NADH (9–11), dehydrogenation of formic acid or alcohols (12, 13), and hydrogenation of organic compounds (14). In these reactions, Rh^{III}–H is believed to be a reactive intermediate (15).

Hydrogen evolution catalysts have been discovered recently in which the metal center and associated ligands cooperate in unexpected ways. A case in point features ligand-centered protonation and subsequent hydride-like reactivity of a nascent C–H bond in a nickel phlorin system (16), although a nickel hydride was not implicated in the cycle for hydrogen evolution. In other work of note, Hull et al. (17) reported dehydrogenation of HCO_2H promoted by proton-responsive hydroxybipyridine-ligated catalysts, and Lacy et al. (18) showed that ligand-centered protonation of a cobalt complex could lead to hydrogen evolution.

Much work has been done on Cp*Rh compounds. Of importance is that Maitlis and coworkers (19) reported Cp*Rh(Cp*H) formation in low yield (14%) by reduction of $[(Cp^*)_2Rh](PF_6)$. In other relevant work, Jones et al. (20) showed that the dihydride complex $Cp^*Rh(PMe_3)(H)_2$ loses free Cp*H on treatment with excess PMe_3 at elevated temperature. Also, several other rhodium and iron complexes with Cp*H ligands are known (21–25).

Building on these earlier investigations, we report here an unusual mode of metal–ligand cooperation that drives proton–hydride tautomerization during hydrogen evolution. We have found that η^4-Cp*H is produced en route to H_2 production with Cp*Rh(diimine) complexes, suggesting an important role for ligand participation in hydrogen evolution catalysis.

Results

The preparation, isolation, and crystallographic characterization of Cp^*Rh^I(diimine) complexes with η^5-Cp* and κ^2-diimine coordination are all well-documented (26, 27). Treatment of the κ^2-2,2′-bipyridyl [bpy; Cp*Rh(bpy); **1**] (Fig. 1) and 1,10-phenanthroline [phen; Cp*Rh(phen); **2**] complexes with excess protonated dimethylformamide ($[DMF{\cdot}H]^+[OTf]^-$) in MeCN ($pK_a = 6.1$) results in stoichiometric production of H_2 gas. Use of weaker acids lowers the thermodynamic driving force for hydrogen evolution (28), likely slowing the reaction and increasing the chance of trapping one or more intermediates. Treatment of **1** with one to five equivalents of $[Et_3NH]^+Br^-$ ($pK_a = 18.8$) in CD_3CN results in a rapid color change

Significance

The discovery of efficient hydrogen evolution catalysts for solar fuels production continues to be an active research field. Catalyst optimization depends on detailed knowledge of the elementary chemical reaction steps involved in catalysis. Isolation of intermediates in catalytic processes is uncommon owing to their necessarily low stability. By using weak acids, we have isolated and characterized an intermediate in the $2e^- + 2H^+ \rightarrow H_2$ reaction catalyzed by η^5-pentamethylcyclopentadienyl (Cp*) Rh(κ^2-2,2′-bipyridyl) [Rh(bpy)]. We find that the preferred site of Cp*Rh(bpy) protonation is not the metal center but is the Cp* ligand. Despite the reputation of Cp* as a stable ligand in organometallic chemistry, these results suggest an important role for close metal–ligand cooperation in promoting hydrogen–evolution catalysis.

Author contributions: S.I.J., D.G.V., J.R.W., H.B.G., and J.D.B. designed research; L.M.A.Q., S.I.J., S.L.C., W.V., M.K.T., and J.D.B. performed research; W.A.G. contributed new reagents/analytic tools; L.M.A.Q., S.I.J., S.L.C., W.V., M.K.T., D.G.V., J.R.W., H.B.G., and J.D.B. analyzed data; and S.I.J., J.R.W., H.B.G., and J.D.B. wrote the paper.

Reviewers: A.M., University of North Carolina; and D.M., The Weizmann Institute of Science.

The authors declare no conflict of interest.

Data deposition: The atomic coordinates and structure factors have been deposited in the Cambridge Crystallographic Data Centre (accession no. 1424707).

[1]To whom correspondence may be addressed. Email: winklerj@caltech.edu, hbgray@caltech.edu, or blakemore@ku.edu.

This article contains supporting information online at www.pnas.org/lookup/suppl/doi:10.1073/pnas.1606018113/-/DCSupplemental.

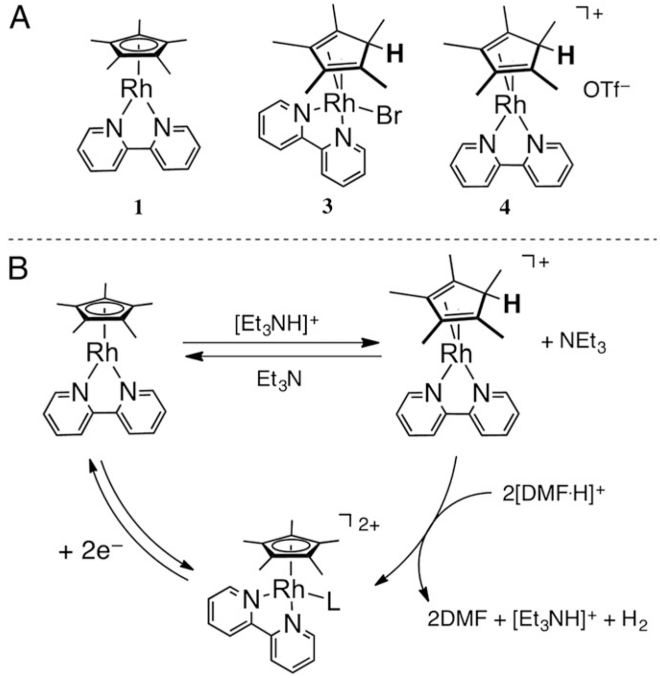

Fig. 1. (*A*) Structures of **1**, **3**, and **4**. (*B*) Proposed cycle for H_2 evolution catalyzed by **1** through a [Cp*H]Rh complex.

from purple to reddish brown but no gas evolution, consistent with formation of compound **3** (Fig. 1). Similar spectral features are encountered on treatment of **1** or **2** with $[Et_3NH]^+OTf^-$, resulting in formation of analogous compounds **4** (with bpy) and **5** (with phen) bearing the [Cp*H] ligand.

Allowing a concentrated acetonitrile solution of **3** to stand for several days yielded orange–yellow single crystals suitable for X-ray diffraction (the structure that we obtained is shown in Fig. 2). The geometry at the Rh^I center is distorted square pyramidal, with a mirror plane containing the Rh1–Br1 bond bisecting the molecule. A proton (observable in the electron density map) is present on the ring of the former Cp* ligand, with the [Cp*H] bound in an η^4 mode. The bpy ligand retains typical κ^2 coordination in accordance with our interpretation of its ^1H and ^{13}C NMR spectra. The Rh1–N1 bond length is 2.117(1) Å, whereas Rh1–C2 and Rh1–C3 are 2.133 (1) and 2.112(2) Å, respectively. The mirror plane symmetry element requires identical bond distances from Rh1 to the corresponding N1′, C2′, and C3′ atoms.[†]

In **1**, the C–C bond length of 1.422(4) Å between the pyridyl rings of the bpy ligand is consistent with considerable bpy anion character (29) caused by electron donation from Rh^I augmented by the strongly π-donating η^5-Cp* ligand. On protonation of Cp* to form **3**, this C–C bond lengthens to 1.475(3) Å, similar to the distance found in free bpy and notably, an analogous $[Cp^*Rh^{III}(bpy)Cl]Cl$ complex (30). This marked structural change is attributable to the conversion of the π-donating $[\eta^5\text{-}Cp^*]^-$ ligand to a π-accepting $[\eta^4\text{-}Cp^*H]^0$ group. In the crystal structure of a free Cp*H analog, $Cp(CH_2Ar)_5H$ [Ar = $-(C_6H_4)CH_3$], the corresponding C2–C3 bond length is 1.343(3) Å, and the C3–C3′ bond is 1.467(3) Å (31). In **3**, the C2–C3 and C3–C3′ bonds are nearly identical at 1.442(2) and 1.442(3) Å, respectively, consistent with both σ-donation and π-backbonding between Rh1 and [Cp*H].

Electronic absorption spectra reflect the marked change in electronic structure on protonation of **1** to form **3**. Bands in the visible region ($\varepsilon \sim 4\text{–}15 \times 10^3\ M^{-1}\ cm^{-1}$) assigned to metal-to-ligand charge-transfer (MLCT) transitions (27, 32) dominate the spectrum of **1**, accounting for its purple color. Conversely, the spectrum of **3** displays intense bands ($\varepsilon \sim 20\text{–}30 \times 10^3\ M^{-1}\ cm^{-1}$) across the UV region with weaker absorption tailing into the visible ($\varepsilon \sim 1.7 \times 10^3\ M^{-1}\ cm^{-1}$ at 507 nm), producing a reddish brown solution. The UV absorption in **3** is attributable to both intraligand and MLCT transitions. The observed blue shift of MLCT absorption bands is consistent with a positive shift of the rhodium(II/I) formal potential on shifting coordination from the electron-donating $[\eta^5\text{-}Cp^*]^-$ ligand to the π-accepting $[\eta^4\text{-}Cp^*H]$ group. Similarly, Rh(norbornadienyl)(bpy)Cl is a reddish solid exhibiting only weak visible absorption ($\varepsilon \sim 0.85 \times 10^3\ M^{-1}\ cm^{-1}$ at 478 nm) (33), and $[Rh(CO)_2(bpy)]ClO_4$ is a yellow solid (34). Because most $[Cp^*Rh^{III}(diimine)L]^{2+}$ complexes are pale yellow to orange in appearance, the coloration of **3** more closely resembles that of an Rh^{III} compound, although it is formally Rh^I (5, 7). This finding raises the possibility that compounds protonated at Cp* may have escaped detection in the past, because their UV-visible absorption profiles are not markedly different from spectra of their hydride analogs.

Exposure of **3**, **4**, and **5** to excess Et_3NH^+ does not lead to additional protonation of the Rh complex or any other transformation. Treatment with stronger acid ($[DMF{\cdot}H]^+[OTf]^-$), however, triggers quantitative H_2 evolution and generation of Rh^{III}. For example, addition of 1 eq $[NEt_3H]^+[OTf]^-$ to 50 mg **2** results in negligible H_2

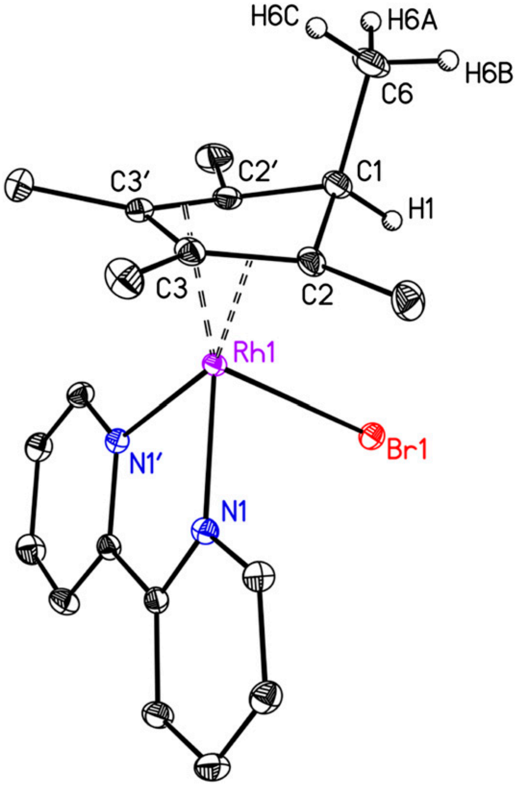

Fig. 2. Structure of **3**. Displacement ellipsoids are shown at 50% probability. One cocrystallized acetonitrile molecule and all H atoms, except those bonded to C1 and C6, are omitted for clarity. Blue, nitrogen; purple, rhodium; red, bromide.

[†] The distinctive ^1H NMR spectrum of **3** is characterized by two singlets in the alkyl region (1.85 and 0.94 ppm) along with a doublet and quartet ($d = 0.54$; $q = 2.54$ ppm; $^3J_{H\text{–}H} = 6.2$ Hz). The relative integrations (6:6:3:1, respectively) of these peak groups are consistent with [Cp*H] coordinated to Rh^I. Resonances in the aromatic region shift on conversion of **1** to **3** but retain the expected couplings for an intact bpy ligand. The remaining features in the ^1H NMR spectrum of **3** are attributed to excess $[Et_3NH]^+Br^-$ and residual CH_3CN. Coordination of [Cp*H] to Rh is confirmed by comparison with the ^1H NMR of the free ligand ($s = 1.74$ and 1.79 ppm; $d = 0.97$; $q = 2.45$ ppm; $^3J_{H\text{–}H} = 7.6$ Hz) as well as the $^{13}C\{^1H\}$ NMR of **3** [$d = 94.4$ ppm; $^1J_{Rh\text{–}C} = 10.6$ Hz; $d = 55.4$ ppm; $^1J_{Rh\text{–}C} = 10.9$ Hz; $d = 57$ ppm; $^2J_{Rh\text{–}C} = 3.6$ Hz; $^{103}Rh(I = 1/2)$ is 100% abundant].

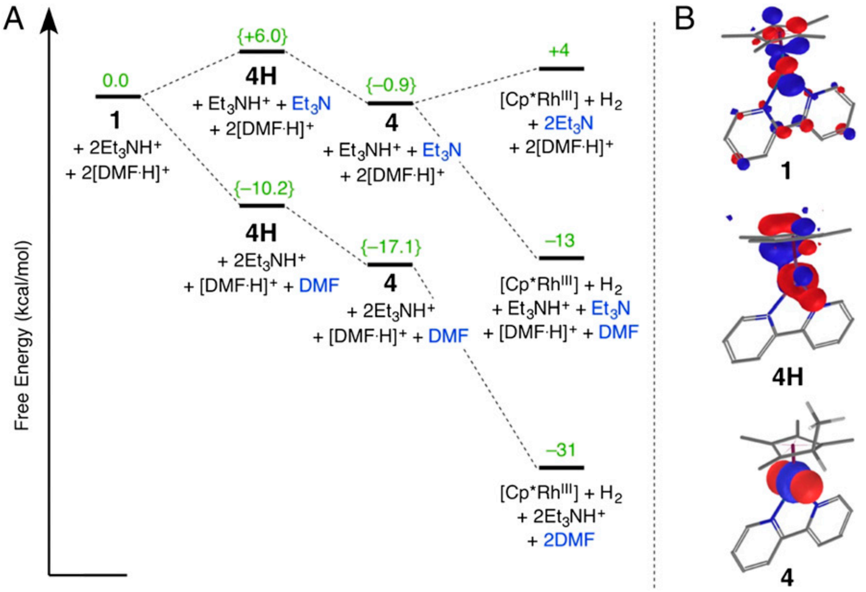

Fig. 3. (*A*) Relative free energies of **1**, its protonated analogs, and net reaction products on H_2 evolution. The lowest energy protonated form **4** bears *endo*-[η^4-Cp*H]. Relative energies are given in green, with modeled values shown in braces and experimental thermodynamic values shown without braces; conjugate bases for the protonation events are given in blue. (*B*) Frontier molecular orbitals computed for compounds **1**, **4H**, and **4**.

production. Addition of 1 eq $[DMF{\cdot}H]^+[OTf]^-$ to the solution containing **5** produces a small yield of H_2 (9%); the predominant reaction is protonation of NEt_3 to form Et_3NH^+. Addition of a second 1 eq $[DMF{\cdot}H]^+[OTf]^-$ results in quantitative formation of H_2 based on remaining Rh^I (91%). The color of the solution at the end of these reactions is pale yellow, consistent with the presence of $[Cp^*Rh^{III}]$. NMR spectra of the reaction products indicate production of H_2 along with resonances for $[Cp^*Rh^{III}]$ complexes with either bound acetonitrile or $[OTf]^-$. Experiments carried out with 1,3,5-$(OMe)_3C_6H_3$ as internal standard confirm >99% final conversion to $[Cp^*Rh^{III}(bpy)]$ complexes. Hydrogen production can be made catalytic by chemical or electrochemical reduction of $[Cp^*Rh^{III}(diimine)]$ to regenerate $[Cp^*Rh^{I}(diimine)]$.

With this knowledge of the observed intermediate in hand, density functional theory (DFT) calculations were carried out for **1**, **4H**, and two tautomeric forms of **4**. Fig. 3*A* shows calculated free energies for these structures and the overall H_2 evolution thermodynamics (values in braces are those calculated by DFT).‡ The upper pathway features protonation of **1** by triethylammonium to form **4**, which is exergonic by ∼1 kcal/mol, whereas formation of the Rh^{III}–H tautomer (**4H**) is endergonic by 6.0 kcal/mol. Complex **4** bears a C–H bond on the Cp* ring, with an unremarkable C–H bond distance computed to be 1.1 Å. Importantly, the Rh to H distance is computed to be 2.86 Å, thus excluding a bridging mode between the metal center and the ring. Another tautomer bearing *exo*-[η^4-Cp*H] (**4X**), in which the ring-bound H faces away from Rh, is slightly less stable (+0.5 kcal/mol) than **4**.

The lower pathway features the same protonated structures formed in reaction with $[DMF{\cdot}H]^+$. The difference between **4** and **4H** is still 6.9 kcal/mol, but the stronger acid increases the free energy released on formation of **4** from **1** to 17.1 kcal/mol. In accordance with experiment, this pathway leads to exergonic evolution of H_2. The free energy changes for the overall reactions are shown in the last column, and they are determined from the experimental $Rh^{III/I}$ reduction potential [−1.05 V vs. a ferricenium/ferrocene ($Fc^{+/0}$) reference] and acid pK_a values of the acids in MeCN (7, 30, 35). Consistent with experimental observations, H_2 evolution using 2 eq $[Et_3NH]^+$ is endergonic, whereas H_2 production with a combination of 1 eq $[Et_3NH]^+$ and 1 eq $[DMF{\cdot}H]^+$ is a spontaneous process.

The frontier molecular orbitals for **1**, **4H**, and **4** are shown in Fig. 3*B*. The ground-state highest occupied molecular orbital (HOMO) of **1** is delocalized onto the ligands (Fig. 3*B*), consistent with the X-ray structure, suggesting significant back donation of electron density from the Rh^I center. On protonation to form **4**, the HOMO shifts to a primarily Rh^I-centered dz^2 orbital stabilized by the newly formed π-accepting [Cp*H] ligand.

Discussion

Based on our experimental data and computational studies, we postulate that reaction of **1** with protic acids initially produces **4H**, which then rearranges to the more stable **4**. Miller and coworkers (36) proposed an analogous pathway involving **4** in the decarboxylation of an Rh^{III} formate complex and most importantly, have directly observed the hydride intermediate by low-temperature protonation of Cp*Rh(bpy). In the work by Miller and coworkers (36), the hydride converts to an η^4-Cp*H complex on warming, a sequence consistent with our observation of exclusive *endo*-protonation of the Cp* ligand. The computed structure of **4H** also features [Cp*] character in the HOMO, providing electron density that would attract H^+ to form **4**.

Deprotonation measurements suggest facile formation and interconversion of **4H** and **4** (as well as analogous **5H**/**5**), but only stronger acids effect the conversion of **3**, **4**, or **5** to H_2 and $[Cp^*Rh^{III}(diamine)]$. With $[NEt_3H]^+[OTf]^-$, hydrogen evolution with **1** or **2** is slightly endergonic based on Rh reduction potentials obtained from cyclic voltammetry (7, 15). However, dissolution of $[Cp^*Rh^{III}(bpy)MeCN][PF_6]_2$ in MeCN containing ∼25 eq NEt_3 under 1 atm H_2 at ambient temperature generates **1** within 30 min, implying low barriers for the individual steps in our reaction sequence.

Two plausible pathways can be envisioned for hydrogen evolution from **4** (Fig. 4). Transient reformation of the monohydride Cp^*Rh^{III}–H (A in Fig. 4) could be followed by protonation at the metal center to produce an $Rh^{III}(H_2)$ complex. Indeed, ^{1}H NMR spectral features suggest the existence of such a hydride species in the case of a bulky κ^2-6,6′-dimethyl-bpy analog (10, 13) or in C_6D_5Cl

---

‡ *SI Appendix* and *Materials and Methods* contain detailed descriptions of computational methods. Experimental thermodynamic values for H_2 evolution are based on published redox potentials (6, 7) and experimental pK_a values.

at 238 K (24). Our isolation and characterization of **4**, however, raise the possibility of an alternative pathway (B in Fig. 4), in which Cp*H serves as a proton relay (37): protonation of **4** at the metal center would form $[(Cp^*H)Rh(H)(bpy)]^{2+}$, which then could evolve H_2 through intramolecular reductive elimination. Protonation of **4** at the Rh center is consistent with the dz^2-localized HOMO identified in DFT calculations. The fact that Et_3NH^+ cannot drive this reaction at low concentrations is attributable to the decreased basicity of **4**; use of stronger acid ($[DMF{\cdot}H]^+$) leads to rapid H_2 generation. The intramolecular reductive elimination mechanism is analogous to pathways proposed to be operative in other highly active H_2 evolution catalysts; the search for experimental evidence for these pathways remains an active area of investigation (38–40).

In our case, [Cp*H] does not dissociate from the metal center, and quantitative H_2 evolution proceeds from the reduced complex (21). Importantly, η^5-Cp* coordination to Rh is restored after hydrogen evolution. The unique properties of the Cp* ligand framework enable π-donor $[\eta^5\text{-}Cp^*]^-$ to convert reversibly to π-acceptor $[\eta^4\text{-}Cp^*H]^0$, stabilizing intermediates in the catalytic cycle. Furthermore, this transformation places a proton tantalizingly close to the metal center (41, 42). For [Cp*Rh] bearing κ^2-(*C,N*)-2-phenylpyridine (ppy), Norton and coworkers (43) have shown that an Rh^{III}–H is the preferred form, likely because of the more electron-rich metal center. However, the $Rh^{III/I}$ $[Cp^*Rh^{III}(ppy)(CH_3CN)^+/Cp^*Rh^{I}(ppy)^-]$ potential in the ppy complex is ~500 mV more negative than that of **1**, resulting in a barrier that prevents H_2-driven production of $[Cp^*Rh(ppy)]^-$ with NEt_3 as base (44).

In Cp*Rh(diimine) complexes, the metal center seems to act as the primary site of proton capture from solution, initially forming a hydride species (**4H**) that we do not directly detect. This hydride then tautomerizes by proton transfer to the nearby basic $[Cp^*]^-$ ligand, restoring the formal Rh^I oxidation state on formation of **4**. This proton–hydride tautomerism represents an interesting analog to proton capture mechanisms in other complexes, such as those described by DuBois and coworkers (38), which rely on pendant amine bases to shuttle protons to the metal center. Our case also contrasts with older reports from Davies et al. (45), Reger et al. (46), and Norton and coworkers (47) involving direct *exo*-transfer of $[H^-]$ to a Cp ligand bound to iron or tungsten complexes.

The pathway of H_2 generation involving initial protonation of complex **4** and subsequent H–H bond formation is reminiscent of bond activation by close metal–ligand cooperation (48), especially those cases involving ligand dearomatization–aromatization processes in pincer-type systems (49). Milstein and coworkers (50) have observed proton transfer to and from a pincer arm in an Ru–H complex, resulting in aromatization–dearomatization of a pyridine core on the ligand. Additionally, in a related example, an Ir complex was suggested to react with D_2 through initial dearomatization of a pincer ligand (51). It follows that the specific organic acid–base used with the complexes described here could affect the energetics and preference of the reaction channel through hydrogen-bonding interactions. In the case of **4**, proton transfer from [Cp*H] to form H_2 would result in aromatization of the [Cp*]; this energetically favorable process lowers the barrier to H–H bond formation.

Hydrogen evolution catalysts must assemble two electrons and two protons into an H_2 molecule. The order in which these four particles are delivered to the catalyst impacts the speed and energetics of the transformation. In the case of $[Cp^*Rh^{III}(\text{diimine})L]^{2+}$ catalysts, the sequence is $e^- + e^- + H^+ + H^+$. Owing to the instability of the Rh^{II} oxidation state, the second electron is delivered at a more positive potential than the first electron. The energetics of subsequent proton delivery, however, follow the usual trend, wherein the first proton can be delivered by a relatively weak acid, but a stronger acid is required to deliver the second proton. After the second proton has been delivered to **4** or **4H**, the complex is poised to facilitate H–H bond formation followed by H_2 dissociation. Our findings provide key insight into the design elements required for a catalyst that avoids deep wells and high barriers in $2e^- + 2H^+$ hydrogen evolution.

Materials and Methods

All manipulations were carried out in a dry N_2-filled glovebox (Vacuum Atmospheres Co.) or under N_2 atmosphere using standard Schlenk techniques unless otherwise noted. All solvents were of commercial grade and dried over activated alumina using a J. C. Meyer Solvent Purification System before use. All chemicals were from major commercial suppliers and used as received without additional purification. ^1H, ^{13}C, and ^{19}F NMR spectra were collected on 400- or 500-MHz Varian or Bruker Spectrometers and referenced to the residual protiosolvent signal (52) in the case of ^1H and ^{13}C or the deuterium lock signal in the case of ^{19}F. Chemical shifts (δ) are reported in units of parts per million, and coupling constants (*J*) are reported in hertz.

Cp*Rh(bpy) and Cp*Rh(phen) were synthesized according to the literature method using Na(Hg)[27]. $[DMF{\cdot}H]^+OTf^-$ was synthesized according to the method by Favier and Duñach (53). $[Et_3NH]^+OTf^-$ was prepared according to the literature (54). The rhodium complexes bearing Cp*H were not isolated in pure form, but instead generated in situ by treatment with triethylammonium salts. ^1H NMR, $^{13}C\{^1H\}$ NMR, and electronic absorption spectroscopy were used to confirm clean conversion of the rhodium starting materials. In one case (**3**), crystals suitable for X-ray diffraction were obtained as described below.

(Cp*)Rh(bpy)Br (3). In a typical experiment, ~5 mg **1** was dissolved in acetonitrile, and then, ~1–5 eq $[Et_3NH]^+Br^-$ was added, resulting in a color change from purple to brown and quantitative formation of **3**. The resulting solution contains **3** plus the conjugate base NEt_3 and any excess $[Et_3NH]^+Br^-$. For NMR analysis, the compound was prepared in d_3-MeCN and transferred to a J. Young Tube. No decomposition of the compound over hours was detectable. However, **3** was prepared fresh for each experiment and typically not isolated as a solid.

Peak multiplicities for the NMR spectra are listed, where d is doublet, q is quartet, s is singlet, dd is doublet of doublets, td is triplet of doublets, t is triplet, and ddd is doublet of doublet of doublets.

^1H NMR (400 MHz; MeCN-d_3) δ 8.88 (d, 2H, $^3J_{H–H}$ = 5.1 Hz), 8.28 (d, 2H, $^3J_{H–H}$ = 8.2 Hz), 8.02 (td, 2H, $^3J_{H–H}$ = 7.9 Hz, $^4J_{H–H}$ = 1.6 Hz), 7.59 (t, 2H, $^3J_{H–H}$ = 6.4 Hz),

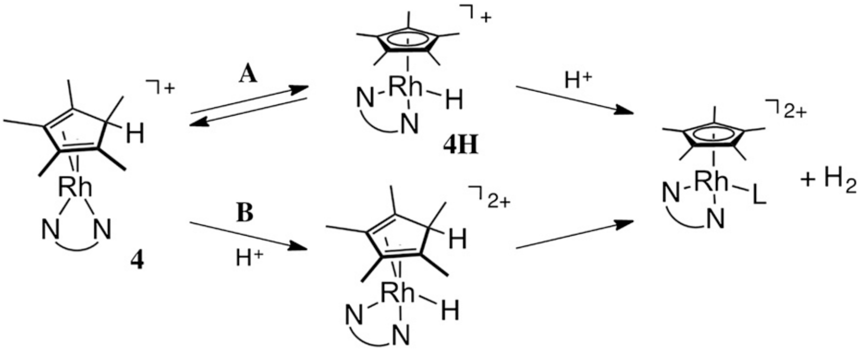

Fig. 4. Proposed pathways for hydrogen evolution starting from **4**.

2.54 (q, 1H, $^3J_{H–H} = 6.2$ Hz), 1.85 (s, 6H), 0.94 (s, 6H), 0.54 (d, 3H, $^3J_{H–H} = 6.2$ Hz). $^{13}C\{^1H\}$ NMR (101 MHz; MeCN-d_3) δ 154.7, 152.2, 138.2, 127.1, 123.2, 94.4 (d, $^1J_{Rh–H}$ = 10.6 Hz), 57.0 (d, $^2J_{Rh–H}$ = 3.6 Hz), 55.4 (d, $^1J_{Rh–H}$ = 10.9 Hz), 19.9, 12.1, 10.7. Electronic absorption (MeCN-d_3): λ_{max} (ε) = 507 nm (1,710 L mol^{-1} cm^{-1}), 351 (8,950), 289 (33,400), 273 (31,500).

Crystals suitable for X-ray diffraction were obtained by allowing a solution of **3** in MeCN to stand at room temperature under inert atmosphere for several days.

(Cp*)Rh(bpy)OTf (4). Compound **4** was prepared analogously to **3** but with $[Et_3NH]^+OTf^-$[; **4** is stable at room temperature for 1–2 h. ^{1}H NMR (400 MHz; MeCN-d_3) δ 8.98 (d, 2H, $^3J_{H–H}$ = 5.0 Hz), 8.36 (d, 2H, $^3J_{H–H}$ = 8.1 Hz), 8.10 (td, 2H, $^3J_{H–H}$ = 7.9 Hz, $^4J_{H–H}$ = 1.7 Hz), 7.67 (ddd, 2H, $^3J_{H–H}$ = 7.6 and 5.3 Hz, $^4J_{H–H}$ = 1.2 Hz), 2.31 (q, 1H, $^3J_{H–H}$ = 6.1 Hz), 1.92 (s, 6H), 0.79 (s, 6H), and 0.53 (d, 3H, $^3J_{H–H}$ = 6.2 Hz). ^{19}F NMR (376 MHz; MeCN-d_3) δ −79.4.

(Cp*)Rh(phen)OTf (5). Compound **5** was prepared analogously to **3** but starting with **2** and $[Et_3NH]^+OTf^-$. ^{1}H NMR (400 MHz; MeCN-d_3) 9.14 (dd, 2H, $^3J_{H–H}$ = 5.0 Hz, $^4J_{H–H}$ = 1.0 Hz), 8.55 (dd, 2H, $^3J_{H–H}$ = 8.1 Hz, $^4J_{H–H}$ = 1.4 Hz), 8.05 (s, 2H), 7.90 (dd, 2H, $^3J_{H–H}$ = 4.9 and 8.2 Hz), 2.47 (q, 1H, $^3J_{H–H}$ = 6.1 Hz), 1.86 (s, 6H), 1.10 (s, 6H), 0.60 (d, 3H, $^3J_{H–H}$ = 6.2 Hz).

X-Ray Crystallography. Low-temperature diffraction data (ϕ- and ω-scans) were collected on a Bruker AXS D8 VENTURE KAPPA Diffractometer coupled to a PHOTON 100 CMOS Detector with Mo K_α radiation (λ = 0.71073 Å) from an IμS Microsource for the structure of compound **3**. The structure was solved by direct methods using SHELXS (55) and refined against F^2 on all data by full-matrix least squares with SHELXL-2014 (56) using established refinement techniques (57). All nonhydrogen atoms were refined anisotropically. Unless otherwise noted, all hydrogen atoms were included in the model at geometrically calculated positions and refined using a riding model. The isotropic displacement parameters of all hydrogen atoms were fixed to 1.2 times the *U* value of the atoms to which they are linked (1.5 times for methyl groups).

Compound **3** crystallizes in the orthorhombic space group *Pnma* with one-half a molecule in the asymmetric unit along with one-half a molecule of acetonitrile. The coordinates for the hydrogen atom bound to C1 were located in the difference Fourier synthesis and refined semifreely with the help of a restraint on the C–H distance [0.98(4) Å].

Cambridge Crystallographic Data Centre accession number 1424707 contains the supplementary crystallographic data for compound **3**. These data can be obtained free of charge at https://summary.ccdc.cam.ac.uk/structure-summary-form or from the Cambridge Crystallographic Data Centre.

GC. Gas analysis for determination of hydrogen evolution on acid addition was performed with an Agilent 7890A Gas Chromatograph with separate columns for analyses of hydrogen gas and nitrogen, oxygen, carbon dioxide, carbon monoxide, hydrogen disulfide, methane, ethane, ethylene, and ethyne. The instrument was calibrated with a standard gas mixture to obtain quantitative data.

For the hydrogen detection experiment, 50 mg **1** or **2** were loaded into an N_2-purged Schlenk flask and dissolved in MeCN. A background experiment before addition of acid confirmed only nitrogen and minimal oxygen in the glovebox atmosphere. Samples of headspace gas were taken after progressive additions of 1 eq $[Et_3NH]^+OTf^-$, 1 eq $[DMF{\cdot}H]^+OTf^-$, and an additional 1 eq $[DMF{\cdot}H]^+OTf^-$.

Computational Details. Geometry, frequency, and solvation calculations were performed with the B3LYP functional (58, 59) with 6–31G** basis set on organics (60, 61). Rh was treated with the Los Alamos Small Core Potential and 2-ζ Basis Set (62). Single-point energy calculations were completed with the M06 functional (63) with the 6–311G**++ basis on organics. Rh was treated with the 3-ζ LACV3P**++ basis set augmented with f and diffuse functions (64). Solvation in acetonitrile was applied using the Poisson Boltzmann polarizable continuum model with a dielectric constant and probe radius of 37.5 and 2.19 Å, respectively. To calculate the free energy of acetonitrile, 1-atm ideal gas free energy was calculated, and the empirical energy of vaporization, 1.27 kcal/mol, was subtracted (65). Free energies were computed from the following equation:

$$G = E_{M06} + G_{solv} + E_{ZPE} + H_{vib} + H_{TR} - T(S_{vib} + S_{elec}),$$

where zero point energies, enthalpic, and entropic effects were provided by frequency calculations at room temperature. To validate calculations with the acids, the pK_a values of triethylammonium and $[DMF{\cdot}H]^+[OTf]^-$ were calculated in acetonitrile. For these calculations, the value of the proton free energy in solution was calculated from its gas-phase free energy ($G_{H+} = H - TS = 2.5k_BT - T \times 26.04 = -6.3$ kcal/mol) plus the empirical free energy of solvation at a concentraion of 1 M [$\Delta G_{H+,solv} = -260.2 + k_BT\ln(24.5)$]. This calculation yields a value of −264.6 kcal/mol (66). Using this method, the pK_a of triethylammonium in acetonitrile was calculated as 17.8, which compares well with the experimentally measured value of 18.8. To obtain a correct pK_a of dimethylformamide in acetonitrile, the van der Waals radii of the acidic proton and basic oxygen were changed to 1.15 and 2.00 Å, respectively. Use of these values, which were published previously (67), produced a calculated pK_a of 5.9, which again compares well with the experimentally measured value of 6.1. In calculations involving the Rh complexes, the acid complexes themselves were used rather than the energy of the free proton. Calculations were completed in Jaguar (68); similarly calculated systems have shown good agreement with experiment (69, 70). In addition, calculated structures were in good agreement with the crystal structures for **1** and **3**, with errors in the Rh–N bond length of ∼0.05 Å and the C–C bond lengths of ∼0.01 Å.

ACKNOWLEDGMENTS. S.I.J. thanks Dr. Robert Nielsen for helpful discussions. This research, which was carried out in part at the Molecular Materials Research Center and the Laser Resource Center of the Beckman Institute (California Institute of Technology), was supported by NSF CCI Solar Fuels Program CHE-1305124. S.I.J. and J.D.B. acknowledge fellowships from the Resnick Sustainability Institute at Caltech.

1. Lewis NS, Nocera DG (2006) Powering the planet: Chemical challenges in solar energy utilization. *Proc Natl Acad Sci USA* 103(43):15729–15735.
2. Halpern J, Peters E (1955) Mechanism of the catalytic activation of molecular hydrogen by metal ions. *J Chem Phys* 23(3):605.
3. Dempsey JL, Winkler JR, Gray HB (2010) Mechanism of H_2 evolution from a photogenerated hydridocobaloxime. *J Am Chem Soc* 132(47):16774–16776.
4. Lacy DC, Roberts GM, Peters JC (2015) The cobalt hydride that never was: Revisiting Schrauzer's "hydridocobaloxime." *J Am Chem Soc* 137(14):4860–4864.
5. Kölle U, Grätzel M (1987) Organometallic rhodium(III) complexes as homogeneous catalysts for the photoreduction of protons to hydrogen on colloidal TiO_2. *Angew Chem Int Ed Engl* 26(6):567–570.
6. Cosnier S, Deronzier A, Vlachopoulos N (1989) Carbon/poly {pyrrole-[(C_5Me_5)Rh(bpy)Cl]$^+$} modified electrodes; a molecularly-based material for hydrogen evolution (bpy = 2,2′-bipyridine). *J Chem Soc Chem Commun* (17):1259–1261.
7. Blakemore JD, Gupta A, Warren JJ, Brunschwig BS, Gray HB (2013) Noncovalent immobilization of electrocatalysts on carbon electrodes for fuel production. *J Am Chem Soc* 135(49):18288–18291.
8. Brintzinger H, Bercaw JE (1971) Bis(pentamethylcyclopentadienyl)titanium(II). Isolation and reactions with hydrogen, nitrogen, and carbon monoxide. *J Am Chem Soc* 93(8):2045–2046.
9. Ruppert R, Herrmann S, Steckhan E (1987) Efficient indirect electrochemical in situ regeneration of NADH: Electrochemically driven enzymatic reduction of pyruvate catalyzed by D-LDH. *Tetrahedron Lett* 28(52):6583–6586.
10. Steckhan E, et al. (1991) Analytical study of a series of substituted (2,2′-bipyridyl)(pentamethylcyclopentadienyl)rhodium and -iridium complexes with regard to their effectiveness as redox catalysts for the indirect electrochemical and chemical reduction of NAD(P)$^+$. *Organometallics* 10(5):1568–1577.
11. Cosnier S, Gunther H (1991) A polypyrrole [$Rh^{III}C_5Me_5$(bpy)Cl]$^+$ modified electrode for the reduction of NAD$^+$ cofactor: Application to the enzymatic reduction of pyruvate. *J Electroanal Chem Interfacial Electrochem* 315(1–2):307–312.
12. Kölle U, Fränzl H (2000) Oxidation of Alcohols by [Cp*Rh(ppy)(OH)]$^+$. *Monatsh Chem* 131(12):1321–1326.
13. Fukuzumi S, Kobayashi T, Suenobu T (2008) Efficient catalytic decomposition of formic acid for the selective generation of H_2 and H/D exchange with a water-soluble rhodium complex in aqueous solution. *ChemSusChem* 1(10):827–834.
14. Blacker AJ, et al. (2009) Synthesis and structure of "16-electron" rhodium(III) catalysts for transfer hydrogenation of a cyclic imine: Mechanistic implications. *Chem Commun (Camb)* 44:6801–6803.
15. Kölle U, Kang BS, Infelta P, Comte P, Grätzel M (1989) Electrochemical and pulse-radiolytic reduction of (pentamethylcyclopentadienyl)(polypyridyl)rhodium complexes. *Chem Ber* 122(10):1869–1880.
16. Solis BH, Maher AG, Dogutan DK, Nocera DG, Hammes-Schiffer S (2016) Nickel phlorin intermediate formed by proton-coupled electron transfer in hydrogen evolution mechanism. *Proc Natl Acad Sci USA* 113(3):485–492.
17. Hull JF, et al. (2012) Reversible hydrogen storage using CO2 and a proton-switchable iridium catalyst in aqueous media under mild temperatures and pressures. *Nat Chem* 4(5):383–388.
18. Lacy DC, McCrory CCL, Peters JC (2014) Studies of cobalt-mediated electrocatalytic CO2 reduction using a redox-active ligand. *Inorg Chem* 53(10):4980–4988.
19. Gusev OV, et al. (1993) Electrochemical generation of 19- and 20-electron rhodocenium complexes and their properties. *J Organomet Chem* 452(1–2):219–222.
20. Jones WD, Kuykendall VL, Selmeczy AD (1991) Ring migration reactions of $(C_5Me_5)Rh(PMe_3)H_2$. Evidence for η^3 slippage and metal-to-ring hydride migration. *Organometallics* 10(5):1577–1586.

21. Macias R, et al. (1997) Effects of metal-centre orbital control on cluster character and electron distribution between borane and hydrocarbon ligands; significance of the structures of $[\mu\text{-9,10-(SMe)-8,8-(PPh}_3)_2\text{-nido-8,7-IrSB}_9\text{H}_9]$ and $[\mu\text{-9,10-(SMe)-8-}(\eta^4\text{-C}_5\text{Me}_5\text{H})\text{-nido-8,7-RhSB}_9\text{H}_9]$. *J Chem Soc Dalton Trans* (2):149–152.
22. Zamorano A, Rendón N, Valpuesta JEV, Álvarez E, Carmona E (2015) Synthesis and reactivity toward H_2 of $(\eta^5\text{-C}_5\text{Me}_5)\text{Rh(III)}$ complexes with bulky aminopyridinate ligands. *Inorg Chem* 54(13):6573–6581.
23. Enders M, et al. (2002) Coordination chemistry of neutral quinolyl- and aminophenylcyclopentadiene derivatives. *J Organomet Chem* 641(1–2):81–89.
24. Tsai W-M, Rausch MD, Rogers RD (1996) Improved synthesis of pentabenzylcyclopentadiene and study of the reaction between pentabenzylcyclopentadiene and iron pentacarbonyl. *Organometallics* 15(11):2591–2594.
25. Liu L-K, Luh L-S (1996) Consecutive butylations on the cyclopentadienyl ring of the $[(\eta^5\text{-C}_5\text{H}_5)\text{Fe(CO)}_2\text{PPh}_3]^+$ cation. *Organometallics* 15(25):5263–5265.
26. Blakemore JD, et al. (2014) Pentamethylcyclopentadienyl rhodium complexes. *Polyhedron* 84:14–18.
27. Nakai H, Jeong K, Matsumoto T, Ogo S (2014) Catalytic C-F bond hydrogenolysis of fluoroaromatics by. *Organometallics* 33(17):4349–4352.
28. Appel AM, Helm ML (2014) Determining the overpotential for a molecular electrocatalyst. *ACS Catal* 4(2):630–633.
29. Gore-Randall E, Irwin M, Denning MS, Goicoechea JM (2009) Synthesis and characterization of alkali-metal salts of 2,2′- and 2,4′-bipyridyl radicals and dianions. *Inorg Chem* 48(17):8304–8316.
30. Dadci L, et al. (1995) π-Arene aqua complexes of cobalt, rhodium, iridium, and ruthenium: Preparation, structure, and kinetics of water exchange and water substitution. *Inorg Chem* 34(1):306–315.
31. Schumann H, Sühring K, Weimann R, Hummert M (2000) Deca(4-methylbenzyl)ferrocene and -stannocene. *Z Naturforsch B* 60(6):527–532.
32. Ladwig M, Kaim W (1992) Electronic structure of catalytic intermediates for production of H_2: $(\text{C}_5\text{Me}_5)\text{Ir(bpy)}$ and its conjugated acid. *J Organomet Chem* 439(1):79–90.
33. Robertson JJ, Kadziola A, Krause RA, Larsen S (1989) Preparation and characterization of four- and five-coordinate rhodium(I) complexes. Crystal structures of chloro(2-phenylazo)pyridine)(norbornadiene)rhodium(I), (2,2′-bipyridyl)(norbornadiene)rhodium(I) chloride hydrate, and chloro(2,2′-bipyridyl)(norbornadiene)rhodium(I). *Inorg Chem* 28(11):2097–2102.
34. Reddy GKN, Susheelamma CH (1970) 2,2′Bipyridyl and o-phenanthroline carbonyl complexes of rhodium. *J Chem Soc D* (1):54.
35. Roberts JAS, Bullock RM (2013) Direct determination of equilibrium potentials for hydrogen oxidation/production by open circuit potential measurements in acetonitrile. *Inorg Chem* 52(7):3823–3835.
36. Pitman CL, Finster ON, Miller AJ (March 7, 2016) Cyclopentadiene-mediated hydride transfer from rhodium complexes. *Chem Commun*, 10.1039/C6CC00575F.
37. Kefalidis CE, et al. (2015) Can a pentamethylcyclopentadienyl ligand act as a proton-relay in f-element chemistry? Insights from a joint experimental/theoretical study. *Dalton Trans* 44(6):2575–2587.
38. Wilson AD, et al. (2006) Hydrogen oxidation and production using nickel-based molecular catalysts with positioned proton relays. *J Am Chem Soc* 128(1):358–366.
39. Jacques P-A, Artero V, Pécaut J, Fontecave M (2009) Cobalt and nickel diimine-dioxime complexes as molecular electrocatalysts for hydrogen evolution with low overvoltages. *Proc Natl Acad Sci USA* 106(49):20627–20632.
40. Solis BH, et al. (2014) Theoretical analysis of cobalt hangman porphyrins: Ligand dearomatization and mechanistic implications for hydrogen evolution. *ACS Catal* 4(12):4516–4526.
41. Helm ML, Stewart MP, Bullock RM, DuBois MR, DuBois DL (2011) A synthetic nickel electrocatalyst with a turnover frequency above 100,000 s^{-1} for H_2 production. *Science* 333(6044):863–866.
42. Solis BH, Yu Y, Hammes-Schiffer S (2013) Effects of ligand modification and protonation on metal oxime hydrogen evolution electrocatalysts. *Inorg Chem* 52(12):6994–6999.
43. Hu Y, et al. (2012) Synthesis, electrochemistry, and reactivity of new iridium(III) and rhodium(III) hydrides. *Organometallics* 31(14):5058–5064.
44. Hu Y, Norton JR (2014) Kinetics and thermodynamics of $\text{H}^-/\text{H}^\bullet/\text{H}^+$ transfer from a rhodium(III) hydride. *J Am Chem Soc* 136(16):5938–5948.
45. Davies SG, Hibberd J, Simpson SJ, Thomas SE, Watts O (1984) Carbon monoxide reduction. Carbonyl(η^5-cyclopentadienyl)hydrido[1,2-bis(diphenylphosphino)ethane]iron: Reactions and formation by reduction of the complex $[(\eta^5\text{-C}_5\text{H}_5)\text{Fe(Ph}_2\text{PCH}_2\text{CH}_2\text{PPh}_2)(\text{CO})]\text{PF}_6$. *J Chem Soc Dalton Trans* (4):701–709.
46. Reger DL, Belmore KA, Atwood JL, Hunter WE (1983) The cis addition of hydride to η^2-alkyne complexes by initial reaction at an η^5-cyclopentadienyl $(\eta^5\text{-C}_5\text{H}_5)$ ring. Crystal and molecular structure of the carbonyl-η^5-cyclopentadienyliron complex $(\eta^5\text{-C}_5\text{H}_5)\text{FeCO(PPh}_3)$. *J Am Chem Soc* 105(17):5710–5711.
47. Bullock RM, Headford CEL, Kegley SE, Norton JR (1985) Hydrogen exchange between the methyl and hydride ligands of dicyclopentadienylhydridomethyltungsten prior to methane elimination. *J Am Chem Soc* 107(3):727–729.
48. Khusnutdinova JR, Milstein D (2015) Metal-ligand cooperation. *Angew Chem Int Ed Engl* 54(42):12236–12273.
49. Zhang J, Leitus G, Ben-David Y, Milstein D (2005) Facile conversion of alcohols into esters and dihydrogen catalyzed by new ruthenium complexes. *J Am Chem Soc* 127(31):10840–10841.
50. Zhang J, Gandelman M, Shimon LJW, Rozenberg H, Milstein D (2004) Electron-rich, bulky ruthenium PNP-type complexes. Acceptorless catalytic alcohol dehydrogenation. *Organometallics* 23(17):4026–4033.
51. Ben-Ari E, Leitus G, Shimon LJW, Milstein D (2006) Metal-ligand cooperation in C-H and H_2 activation by an electron-rich PNP Ir(I) system: Facile ligand dearomatization-aromatization as key steps. *J Am Chem Soc* 128(48):15390–15391.
52. Fulmer GR, et al. (2010) NMR chemical shifts of trace impurities: Common laboratory solvents, organics, and gases in deuterated solvents relevant to the organometallic chemist. *Organometallics* 29(9):2176–2179.
53. Favier I, Duñach E (2004) New protic salts of aprotic polar solvents. *Tetrahedron Lett* 45(17):3393–3395.
54. Fumino K, Fossog V, Wittler K, Hempelmann R, Ludwig R (2013) Dissecting anion-cation interaction energies in protic ionic liquids. *Angew Chem Int Ed Engl* 52(8):2368–2372.
55. Sheldrick GM (1990) Phase annealing in SHELX-90: Direct methods for larger structures. *Acta Crystallogr A* 46(6):467–473.
56. Sheldrick GM (2008) A short history of SHELX. *Acta Crystallogr A* 64(Pt 1):112–122.
57. Müller P (2009) Practical suggestions for better crystal structures. *Crystallogr Rev* 15(1):57–83.
58. Becke AD (1993) Density-functional thermochemistry. III. The role of exact exchange. *J Chem Phys* 98(7):5648–5652.
59. Lee C, Yang W, Parr RG (1988) Development of the Colle-Salvetti correlation-energy formula into a functional of the electron density. *Phys Rev B Condens Matter* 37(2):785–789.
60. Francl MM, et al. (1982) Self-consistent molecular orbital methods. XXIII. A polarization-type basis set for second-row elements. *J Chem Phys* 77(7):3654–3665.
61. Hehre WJ, Ditchfield R, Pople JA (1972) Self-consistent molecular orbital methods. XII. Further extensions of Gaussian-type basis sets for use in molecular orbital studies of organic molecules. *J Chem Phys* 56(5):2257–2261.
62. Hay PJ, Wadt WR (1985) Ab initio effective core potentials for molecular calculations. Potentials for potassium to gold including the outermost core orbitals. *J Chem Phys* 82(1):299–310.
63. Zhao Y, Truhlar DG (2008) The M06 suite of density functionals for main group thermochemistry, thermochemical kinetics, noncovalent interactions, excited states, and transition elements: Two new functionals and systematic testing of four M06-class functionals and 12 other functionals. *Theor Chem Acc* 120(1-3):215–241.
64. Martin JML, Sundermann A (2001) Correlation consistent valence basis sets for use with the Stuttgart-Dresden-Bonn relativistic effective core potentials: The atoms Ga-Kr and In-Xe. *J Chem Phys* 114(8):3408–3420.
65. Bridgeman OC, Aldrich EW (1964) Vapor pressure tables for water. *J Heat Transfer* 86(2):279–286.
66. Kelly CP, Cramer CJ, Truhlar DG (2007) Single-ion solvation free energies and the normal hydrogen electrode potential in methanol, acetonitrile, and dimethyl sulfoxide. *J Phys Chem B* 111(2):408–422.
67. Lam YC, Nielsen RJ, Gray HB, Goddard WA (2015) A Mn bipyrimidine catalyst predicted to reduce CO2 at lower overpotential. *ACS Catal* 5(4):2521–2528.
68. Bochevarov AD, et al. (2013) Jaguar: A high-performance quantum chemistry software program with strengths in life and materials sciences. *Int J Quantum Chem* 113(18):2110–2142.
69. Zhao Y, Truhlar DG (2009) Benchmark energetic data in a model system for Grubbs II Metathesis Catalysis and Their Use for the Development, Assessment, and Validation of electronic structure methods. *J Chem Theory Comput* 5(2):324–333.
70. Young KJH, et al. (2011) Synthesis of osmium and ruthenium complexes bearing dimethyl (S,S)-2,2′-(pyridine-2,6-diyl)-bis-(4,5-dihydrooxazol-4-carboxylate) ligand and application to catalytic H/D exchange. *J Mol Catal A: Chem* 339(1-2):17–23.